

ADVANCED DEEP NETWORKS FOR 3D MITOCHONDRIA INSTANCE SEGMENTATION

Mingxing Li, Chang Chen, Xiaoyu Liu, Wei Huang, Yueyi Zhang, Zhiwei Xiong[†]
University of Science and Technology of China

ABSTRACT

Mitochondria instance segmentation from electron microscopy (EM) images has seen notable progress since the introduction of deep learning methods. In this paper, we propose two advanced deep networks, named Res-UNet-R and Res-UNet-H, for 3D mitochondria instance segmentation from Rat and Human samples. Specifically, we design a simple yet effective anisotropic convolution block and deploy a multi-scale training strategy, which together boost the segmentation performance. Moreover, we enhance the generalizability of the trained models on the test set by adding a denoising operation as pre-processing. In the Large-scale 3D Mitochondria Instance Segmentation Challenge at ISBI 2021, our method ranks the 1st place. Code is available in the supplementary material and also publicly released.

Index Terms— Electron microscopy, mitochondria, instance segmentation, deep network

1. INTRODUCTION

As an important kind of organelle, mitochondria provide energy for cells and are of great value to the research of life science. Generally, electron microscopy (EM) images that contain recognizable mitochondria consume a huge storage, e.g., at the scale of Terabyte [1]. Manual instance segmentation of mitochondria from such a large amount of data is impossible, and automatic segmentation algorithms are highly desired. As pioneer works, Lucci et al. [2] propose a supervoxel-based method with learned shape features to recognize mitochondria. Seyedhosseini et al. [3] use algebraic curves and a random forest classifier to segment mitochondria. Due to the limited generalizability, however, these traditional methods cannot be easily adapted to large-scale datasets such as MitoEM [4] including both rat and human samples.

Recently, some methods based on convolutional neural networks (CNNs) have emerged for mitochondrial segmentation. For example, Oztel et al.[5] propose a deep network to segment 2D mitochondria slices first and then integrate 3D information with median filtering in the axial dimension. Wei et al. [4] summarize the CNN-based methods into two groups,

top-down methods and bottom-up methods. Representative top-down methods use Mask-RCNN [6] for instance segmentation. Due to the elongated and distorted shape of mitochondria, however, it is difficult to set a proper anchor size for Mask-RCNN in this task. The bottom-up methods usually predict a binary segmentation mask [7], an affinity map [8], or a binary mask with the instance boundary [9]. Then a post-processing algorithm is used to distinguish instances. Although notable progress has been achieved, there is still a large room for improving the performance of mitochondria instance segmentation.

In this paper, we propose two advanced deep residual networks, named Res-UNet-R for the rat sample and Res-UNet-H for the human sample on the MitoEM dataset. Both networks generate the same form of outputs, including a semantic mask and an instance boundary. Since the human sample is more difficult (i.e., containing more noise) than the rat sample, we increase a decoder path for Res-UNet-H to predict the semantic mask and the instance boundary separately, while the decoder of Res-UNet-R has only one path. Obtaining the semantic mask and the instance boundary, we then synthesize a seed map. Finally, we adopt the connected component labeling to obtain the mitochondria instances.

To boost the segmentation performance of our networks, we design a simple yet effective anisotropic convolution block and deploy a multi-scale training strategy. Moreover, we observe that imaging noise is sparsely distributed on the MitoEM dataset. Especially in the human sample, the noise level is subjectively stronger than that in the rat sample. To alleviate the influence of noise on segmentation, we utilize an interpolation network [10, 11] to restore the noisy regions coarsely marked by labor. In addition to mitochondria instance segmentation, we also verify the proposed method has superior performance for mitochondria semantic segmentation.

2. METHOD

2.1. Res-UNet-R and Res-UNet-H

We follow the bottom-up methods to extract the response map of mitochondria first. For the rat sample and the human sample, we propose two deep residual networks named Res-UNet-R and Res-UNet-H respectively. In the following description, we omit the exponential linear unit (ELU) after the convolutional layer for brevity.

This work has been submitted to the IEEE for possible publication. Copyright may be transferred without notice, after which this version may no longer be accessible. [†] Correspondence should be addressed to zwxiong@ustc.edu.cn

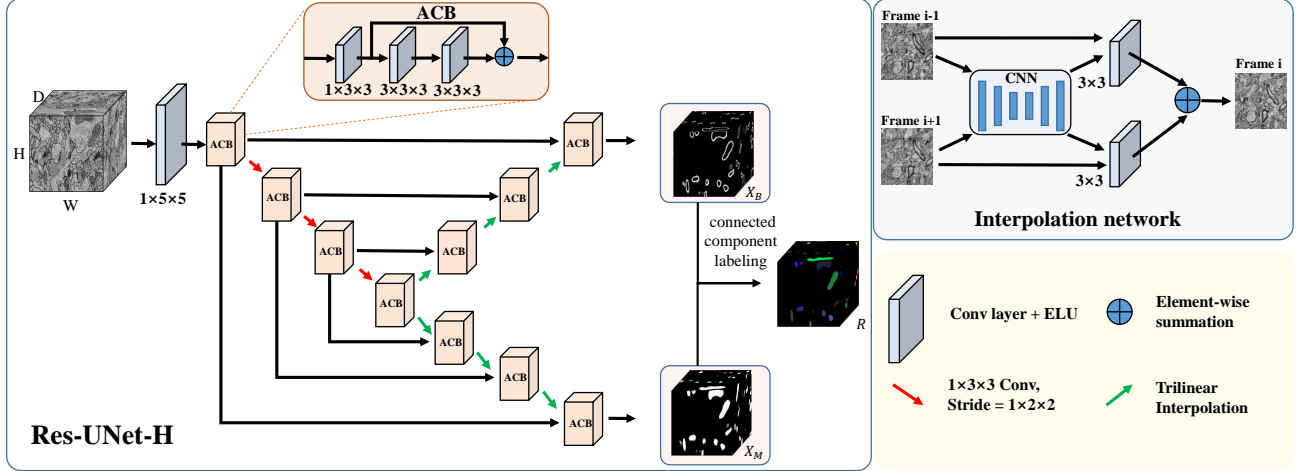


Fig. 1. Network structure of Res-UNet-H. Note the decoder of Res-UNet-R has only one path to generate the semantic mask and the instance boundary simultaneously.

Anisotropic Convolution Block. Since the MitoEM dataset has anisotropic resolution, we design an anisotropic convolution block (ACB) as shown in Fig. 1. After a $1 \times 3 \times 3$ conventional layer, we cascade two $3 \times 3 \times 3$ conventional layers to further enlarge the receptive field. At the same time, we insert the skip connection in the two $3 \times 3 \times 3$ conventional layers.

Network Structure. The overall structure of Res-UNet-H is shown in Fig. 1. Inspired by 3D U-Net [12], we first embed the feature maps extracted from a 3D block with a $1 \times 5 \times 5$ convolutional layer. In each layer of the encoder, there is an ACB to extract the anisotropic information. Then we adopt a $1 \times 3 \times 3$ convolutional layer to downsample the feature maps in the lateral dimensions. In the decoder, we use the trilinear upsampling to restore the resolution of the feature maps and the ACB to reconstruct the detailed information. For Res-UNet-R, the decoder outputs a semantic mask and an instance boundary simultaneously. Since the human sample is of poorer imaging quality than the rat sample, we design two decoder paths for Res-UNet-H to predict the semantic mask and the instance boundary separately.

Loss Function. The binary cross entropy (BCE) is a common loss function used in biomedical image segmentation. To address the class imbalance problem, we adopt a weighted BCE (WBCE) loss as

$$L_{WBCE}(\mathbf{X}_i, \mathbf{Y}_i) = \frac{1}{DHW} \mathbf{W}_i L_{BCE}(\mathbf{X}_i, \mathbf{Y}_i), \quad (1)$$

where \mathbf{X}_i and \mathbf{Y}_i are the predicted response map and ground-truth of the i -th block, D , H , and W denote the depth, height, and width of the block, and the weight \mathbf{W}_i is defined as

$$\mathbf{W}_i = \begin{cases} \mathbf{Y}_i + \frac{W_f}{1-W_f}(1 - \mathbf{Y}_i) & W_f > 0.5 \\ \frac{1-W_f}{W_f} \mathbf{Y}_i + (1 - \mathbf{Y}_i) & else \end{cases} \quad (2)$$

Here W_f is the foreground voxel ratio, i.e., $W_f = \frac{\text{sum}(\mathbf{Y}_i)}{DHW}$.

The overall loss function L is defined as

$$L = L_{WBCE}(\mathbf{X}_M, \mathbf{Y}_M) + L_{WBCE}(\mathbf{X}_B, \mathbf{Y}_B), \quad (3)$$

where \mathbf{X}_M and \mathbf{X}_B are the predicted response maps of the semantic mask and the instance boundary respectively. \mathbf{Y}_M and \mathbf{Y}_B are the corresponding ground-truth of \mathbf{X}_M and \mathbf{X}_B .

2.2. Post-processing

Obtaining the semantic mask $\mathbf{X}_M \in \mathbb{R}^{D \times H \times W}$ and the instance boundary $\mathbf{X}_B \in \mathbb{R}^{D \times H \times W}$, we can generate the seed map $\mathcal{S}^j (j \in [1, D \times H \times W])$ as

$$\mathcal{S}^j = \begin{cases} 1 & \mathbf{X}_M^j > T_1, \mathbf{X}_B^j < T_2 \\ 0 & else \end{cases} \quad (4)$$

where T_1 and T_2 are two thresholds. In our experiments, we set $T_1 = 0.9$ and $T_2 = 0.8$. Then we generate the seed map and adopt the connected component labeling to obtain the final mitochondria instances.

2.3. Denoising as Pre-processing

As mentioned above, we find that by adding a denoising operation as pre-processing on the test set, the influence of noisy regions on segmentation can be alleviated, especially for the human sample. To this end, we adopt the interpolation network initially proposed for video frame [10] and also employed for EM image restoration in [11]. As shown in Fig. 1, the interpolation network takes the two adjacent frames of the noisy frame as input and predicts two kernels. The two adjacent frames are then convolved by the two kernels respectively, the sum of which contributes to the restored frame.

3. EXPERIMENTS

3.1. Dataset

The MitoEM dataset [4] consists of two $(30 \mu m)^3$ EM image volumes of resolution $8 \times 8 \times 30 nm$, which come from a rat tissue (MitoEM-R) and a human tissue (MitoEM-H) respectively. Each tissue has three parts, a training set ($400 \times 4096 \times 4096$), a validation set ($100 \times 4096 \times 4096$) and a test set ($500 \times 4096 \times 4096$). Lucchi [2] is a mitochondria semantic segmentation dataset in which the training and test data volumes are with a size of $165 \times 1024 \times 768$.

3.2. Implementation Details

We adopt Pytorch (version 1.1) to implement the proposed method. Two TITAN Xp (12GB) are used for training and inference. For the MitoEM dataset, during the training stage, we adopt the data augmentation methods following [4] and set the batch size as 2. The network is optimized by Adam with a fixed learning rate 0.0001. We train the network in two stages. First, we train the network in 20K iterations with the input size $32 \times 256 \times 256$ to select the best model. Then we change the input size to $36 \times 320 \times 320$ and fine-tune the network in 10K iterations. We call this two-stage training as multi-scale training (MT). The training and inference details of interpolation network can be found in the supplementary material. For the Lucchi dataset, we train Res-UNet-R with only the semantic mask output, following the training details in [4]. Connected component labeling is no longer needed for the semantic segmentation task.

3.3. Evaluation Metrics and Results

We adopt an efficient 3D AP-75 metric [4] on the MitoEM dataset. In this case, at least 0.75 intersection over union

Method	MitoEM-R	MitoEM-H
Wei [4]	0.521	0.605
Nightingale [13]	0.715	0.625
Li [14]	0.870	0.787
Ours	0.917	0.828

Table 1. Instance segmentation results on the MitoEM validation set.

Method	Jaccard	DSC
Lucchi [15]	0.755	0.860
Liu [16]	0.864	0.926
Yuan [17]	0.865	0.927
Wei [4]	0.887	-
Casser [?]	0.890	0.942
Res-UNet-R	0.895	0.945

Table 2. Semantic segmentation results on the Lucchi test set.

(IoU) with the ground truth for a detection is required to be a true positive (TP). According to the number of mitochondrial voxels, mitochondria are divided into small, medium and large instances, with respective thresholds of 5K and 15K. On the Lucchi dataset, we evaluate jaccard-index coefficient (jaccard) and dice similarity coefficient (DSC) for the foreground objects in the volumes.

As shown in Table 1, on the MitoEM validation set, the AP-75 of the proposed method surpasses the existing deep learning-based methods, Wei [4], Nightingale [13] and Li [14], by a large margin. Besides, for the semantic segmentation dataset Lucchi, the proposed method also outperforms some recent competitors, e.g., Lucchi [15], Liu [16], Yuan [17], Wei [4] and Casser [?] as shown in Table 2.

3.4. Ablation Study

Main components. Take Res-UNet-R as an example, the simple baseline only generates the semantic mask and uses 3D Res block without the MT strategy. The proposed method adopts instance boundary and uses 3D ACB block with the MT strategy. We conduct an ablation study for the three main components in Table 3, which validates their effectiveness. In the following subsections, we show more details about the different components and strategies.

Block Unit Selection. We test different block units in Table 4 on the validation set of MitoEM-R. Here 3D SE block [18], 3D ECA block [19] and 3D Res block [20] are simply modified from state-of-the-art methods for the image recognition task. In comparison with these more complex block units, our simply designed ACB alleviates overfitting and achieves the best results on the 3D mitochondria instance segmentation task.

Network Structure. As shown in Table 5, if we train and test Res-UNet-R on MitoEM-H, the AP-75 result is 0.783. By introducing an extra decoder, Res-UNet-H improves the AP-75 result to 0.816 (3.3% increment). It verifies that Res-UNet-H can handle more complex samples.

Training Strategy. As shown in Table 3 and 5, the multi-scale training strategy (MT) we used is beneficial for both models, especially for Res-UNet-H (AP-75 improves 1.2%). It proves that both models need larger receptive field to avoid over-fitting.

Denosing Pre-processing. As shown in Fig. 3, the noisy

Instance boundary	ACB	MT	MitoEM-R			
			Small	Med	Large	ALL
×	×	×	0.210	0.364	0.761	0.623
✓	×	×	0.240	0.832	0.870	0.845
✓	✓	×	0.307	0.853	0.935	0.913
✓	✓	✓	0.277	0.850	0.949	0.917

Table 3. Ablation of main components on the MitoEM-R validation set.

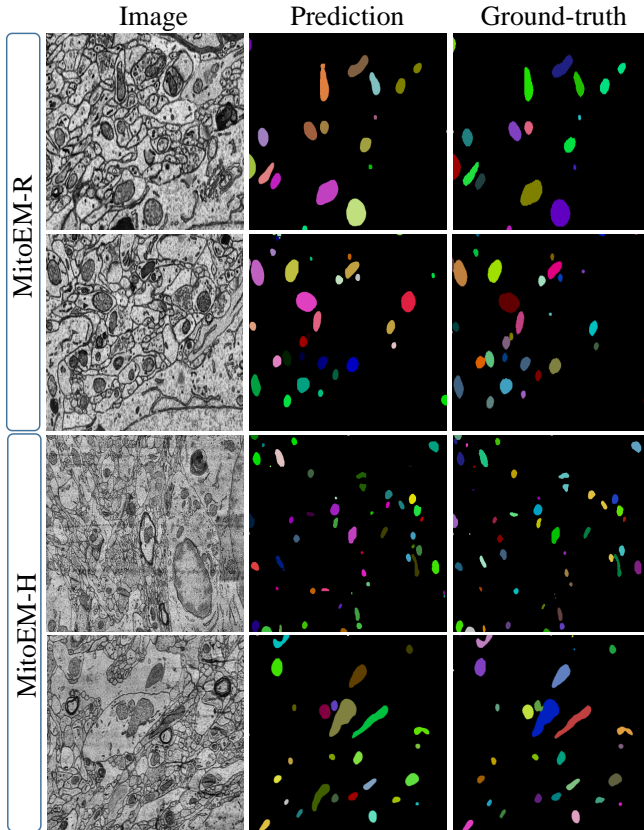


Fig. 2. Visualized results on the MitoEM validation set.

Block unit	MitoEM-R			
	Small	Med	Large	ALL
2D Res block	0.240	0.832	0.870	0.845
3D ECA block	0.398	0.831	0.874	0.865
3D SE block	0.388	0.826	0.891	0.872
3D Res block	0.375	0.860	0.901	0.884
3D ACB	0.307	0.853	0.935	0.913

Table 4. Ablation of block unit selection on the MitoEM-R validation set.

Method	MitoEM-H			
	Small	Med	Large	ALL
Res-UNet-R	0.470	0.791	0.790	0.783
Res-UNet-H	0.405	0.805	0.837	0.816
Res-UNet-H+MT	0.522	0.844	0.826	0.828

Table 5. Ablation of network structure on the MitoEM-H validation set.

regions of the middle frame can be well restored by the interpolation network. As shown in Table 6, it is demonstrated that the generalizability of the trained models can be enhanced on the test set by adding this denoising operation as pre-processing.

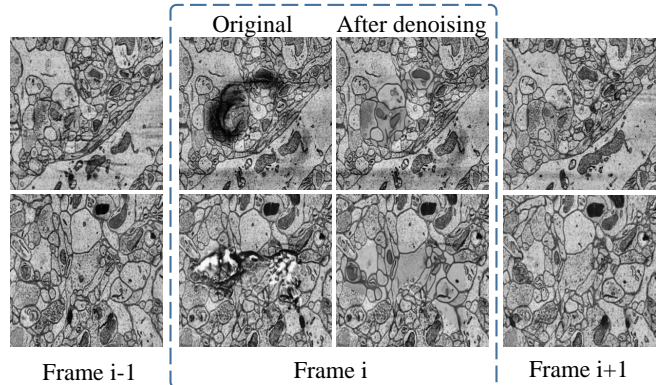


Fig. 3. Visualized results before and after denoising pre-processing on the MitoEM-H test set.

Method	MitoEM-R			
	Small	Med	Large	ALL
Res-UNet-R	0.305	0.861	0.848	0.850
After denoising	0.151	0.832	0.854	0.851
Method	MitoEM-H			
	Small	Med	Large	ALL
Res-UNet-H	0.522	0.844	0.826	0.828
After denoising	0.531	0.834	0.827	0.829

Table 6. Ablation of denoising pre-processing on the MitoEM test set.

Method	MitoEM-R	MitoEM-H	Average
Ours	0.851	0.829	0.8400
2nd	0.836	0.800	0.8180
3rd	0.833	0.800	0.8165
4th	0.816	0.804	0.8100

Table 7. MitoEM Challenge leaderboard at the end of the testing phase.

3.5. Challenge Results

In the Large-scale 3D Mitochondria Instance Segmentation Challenge at ISBI 2021, our method ranks the 1st place. As shown in Table 7, the proposed method notably outperforms other competitors on both MitoEM-R and MitoEM-H test sets. We also show some visualized results from the validation set of MitoEM-R and MitoEM-H in Fig.2. It can be seen that the predicted results by the proposed method is very close to ground-truth.

4. CONCLUSION

In this paper, we present two advanced deep networks for 3D mitochondria instance segmentation, named Res-UNet-R for the rat sample and Res-UNet-H for the human sample. Specifically, we exploit a simple yet effective ACB and a multi-scale training strategy to boost the segmentation performance. Moreover, we enhance the generalizability of the trained models on the test set by adding a denoising operation as pre-processing.

tion as pre-processing. Experimental results demonstrate that the proposed method not only significantly outperforms existing solutions for mitochondria instance segmentation, but also has superior performance for mitochondria semantic segmentation.

5. REFERENCES

- [1] Alessandro Motta et al., “Dense connectomic reconstruction in layer 4 of the somatosensory cortex,” *Science*, vol. 366, no. 6469, 2019.
- [2] Aurélien Lucchi et al., “Supervoxel-based segmentation of mitochondria in em image stacks with learned shape features,” *IEEE transactions on medical imaging*, vol. 31, no. 2, pp. 474–486, 2011.
- [3] Mojtaba Seyedhosseini, Mark H Ellisman, and Tolga Tasdizen, “Segmentation of mitochondria in electron microscopy images using algebraic curves,” in *ISBI*, 2013.
- [4] Donglai Wei, Zudi Lin, et al., “Mitoem dataset: Large-scale 3d mitochondria instance segmentation from em images,” in *MICCAI*, 2020.
- [5] Ismail Oztel, Gozde Yolcu, Ilker Ersoy, Tommi White, and Filiz Bunyak, “Mitochondria segmentation in electron microscopy volumes using deep convolutional neural network,” in *BIBM*, 2017.
- [6] Kaiming He, Georgia Gkioxari, Piotr Dollár, and Ross Girshick, “Mask r-cnn,” in *ICCV*, 2017.
- [7] Olaf Ronneberger, Philipp Fischer, and Thomas Brox, “U-net: Convolutional networks for biomedical image segmentation,” in *MICCAI*, 2015.
- [8] Kisuk Lee, Jonathan Zung, Peter Li, Viren Jain, and H Sebastian Seung, “Superhuman accuracy on the snemi3d connectomics challenge,” *arXiv preprint arXiv:1706.00120*, 2017.
- [9] Hao Chen, Xiaojuan Qi, Lequan Yu, and Pheng-Ann Heng, “Dcan: deep contour-aware networks for accurate gland segmentation,” in *CVPR*, 2016.
- [10] Simon Niklaus, Long Mai, and Feng Liu, “Video frame interpolation via adaptive convolution,” in *CVPR*, 2017.
- [11] Wei Huang, Chang Chen, Zhiwei Xiong, Yueyi Zhang, Dong Liu, and Feng Wu, “Learning to restore sstem images from deformation and corruption,” in *ECCV*, 2020.
- [12] Özgün Çiçek et al., “3d u-net: learning dense volumetric segmentation from sparse annotation,” in *MICCAI*, 2016.
- [13] Luke Nightingale, Joost de Folter, Helen Spiers, Amy Strange, Lucy M Collinson, and Martin L Jones, “Automatic instance segmentation of mitochondria in electron microscopy data,” *bioRxiv*, 2021.
- [14] Zhili Li, Xuejin Chen, Jie Zhao, and Zhiwei Xiong, “Contrastive learning for mitochondria segmentation,” *arXiv preprint arXiv:2109.12363*, 2021.
- [15] Aurélien Lucchi, Yunpeng Li, and Pascal Fua, “Learning for structured prediction using approximate subgradient descent with working sets,” in *CVPR*, 2013.
- [16] Jing Liu, Linlin Li, Yang Yang, Bei Hong, Xi Chen, Qiwei Xie, and Hua Han, “Automatic reconstruction of mitochondria and endoplasmic reticulum in electron microscopy volumes by deep learning,” *Frontiers in neuroscience*, vol. 14, pp. 599, 2020.
- [17] Zhimin Yuan, Jiajin Yi, Zhengrong Luo, Zhongdao Jia, and Jialin Peng, “Em-net: Centerline-aware mitochondria segmentation in em images via hierarchical view-ensemble convolutional network,” in *ISBI*, 2020.
- [18] Jie Hu, Li Shen, and Gang Sun, “Squeeze-and-excitation networks,” in *CVPR*, 2018.
- [19] Qilong Wang et al., “Eca-net: Efficient channel attention for deep convolutional neural networks,” in *CVPR*, 2020.
- [20] Kaiming He, Xiangyu Zhang, Shaoqing Ren, and Jian Sun, “Deep residual learning for image recognition,” in *CVPR*, 2016.